Conductance Switching of Azobenzene-Based Self-Assembled Monolayers on Cobalt Probed by UHV Conductive-AFM.

Louis Thomas,[1,#] Imane Arbouch,[2,#] David Guérin,[1] Xavier Wallart,[1] Colin van Dyck,[2] Thierry Mélin,[1] Jérôme Cornil,[2,*] Dominique Vuillaume[1,*] and Stéphane Lenfant[1,*]

1) Institute of Electronics Microelectronics and Nanotechnology (IEMN), CNRS, University of Lille, Avenue Poincaré, Villeneuve d'Ascq, France.

2) Laboratory for Chemistry of Novel Materials, University of Mons, Place du Parc 20, Mons, Belgium.

Supporting Information

1. XPS characterization.

High resolution XPS spectra were recorded with a monochromatic $Al_{K\alpha}$ X-ray source ($h\upsilon$ = 1486.6 eV), a detection angle of 45° as referenced to the sample surface, an analyzer entrance slit width of 400 µm and with an analyzer pass energy of 12 eV. In these conditions, the overall resolution as measured from the full-width half-maximum (FWHM) of the Ag $3d_{5/2}$ line is 0.55 eV. Background was subtracted by the Shirley method.[1] The peaks were decomposed using Voigt functions and a least squares minimization procedure.

2. Ellipsometry.

The system acquired a spectrum ranging from 2 to 4.5 eV (corresponding to 300 to 750 nm) with intervals of 0.1 eV (or 15 nm). To use the cell filled with N_2, data were taken at an angle of incidence of

60 ± 1° while the compensator was set at 45°. We fitted the data with DeltaPsi 2 data analysis software by a regression analysis to a film on a substrate model as described by their thickness and their complex refractive indexes. First, we recorded a background before monolayer deposition for a cobalt substrate freshly evaporated on the silicon substrate. We acquired three reference spectra at three different places of the surface spaced of few mm. Secondly, after the monolayer deposition, we acquired once again three spectra at three different places of the surface. We used a 2-layer model (substrate/SAM) to fit the measured data and to determine the SAM thickness. We used the previously measured optical properties of the cobalt substrate (background) and we fixed the refractive index of the organic monolayer at 1.50. The usual values in the literature for the refractive index of organic monolayers are in the range 1.45-1.50.[2, 3] The three spectra measured on the sample were fitted separately using each of the three reference spectra, giving nine values for the SAM thickness. We calculated the mean value from this nine thickness values and the thickness incertitude corresponding to the standard deviation.

3. CAFM measurements.

CAFM imaging and local current-voltage (I-V) spectroscopy were carried out using Platinum-Iridium coated probes SCM-PIC-V2 (Bruker), tip radius R = 25 nm, spring constant k = 0.1 N/m. In all our measurements, bias (V) was applied on the substrate and the current was recorded with an external DLPCA-200 amplifier (FEMTO) at a gain of 1µA/V, which set the current sensitivity limit at ca. 10^{-10} A. The force applied on the sample by the tip was calculated from approach-retract curves prior to each experiment to ensure the correct vertical deflection set point with respect to the fixed force set point (F). The load force was set at ~ 20 nN for all the *I-V* measurements, a lower value leading to too many contact instabilities during the *I-V* measurements. Albeit larger than the usual load force (2-5 nN) used

for CAFM on SAMs, this value is below the limit of about 60-70 nN at which the SAMs start to suffer from severe degradations. For example, a detailed study (Ref. 4) showed a limited strain-induced deformation of the monolayer (≤ 0.3 nm) at this used load force. The same conclusion was confirmed by our own study comparing mechanical and electrical properties of alkylthiol SAMs on flat Au surfaces and tiny Au nanodots.[5] Moreover, we checked by topographic AFM that a load force of 20 nN is not indenting the SAM.[6] Current-voltage spectra (I-V) were acquired on several grids (20 x 20 points spaced by 25 nm from each other), each grid spaced of a few mm. Data were processed using Gwyddion[7] and WSxM[8] software. We typically recorded 1200 I-V traces, used without data selection to construct 2D histogram of the decimal logarithm of the current versus voltage. For a given bias, we fitted the current histogram with log-normal distributions and extracted the relevant statistical quantities: the log-mean current (log-μ) and the log-standard deviation (log-σ). Topographic and current images (at a given bias) were also recorded simultaneously. As usually reported in literature[4, 9-11] the contact radius (a) between the C-AFM tip and the SAM surface, and the SAM elastic deformation (δ) are estimated from a Hertzian model:[12]

$$a^2 = \left(\frac{3RF}{4E^*} \right)^{2/3} \tag{S1}$$

$$\delta = \left(\frac{9}{16R} \right)^{1/3} \left(\frac{F}{E^*} \right)^{2/3} \tag{S2}$$

with F the tip load force (20 nN), R the tip radius (25 nm) and E* the reduced effective Young modulus defined as:

$$E^* = \left(\frac{1}{E^*_{SAM}} + \frac{1}{E^*_{tip}} \right)^{-1} = \left(\frac{1-\nu^2_{SAM}}{E_{SAM}} + \frac{1-\nu^2_{tip}}{E_{tip}} \right)^{-1} \tag{S3}$$

In this equation, $E_{SAM/tip}$ and $\nu_{SAM/tip}$ are the Young modulus and the Poisson ratio of the SAM and C-AFM tip, respectively. For the Pt/Ir (90%/10%) tip, we have E_{tip} = 204 GPa and $\nu_{SAM/tip}$ = 0.37 using a rule of mixture with the known material data.[13] These parameters for the AzBT SAM are not known and, in general, they are not easily determined in such a monolayer material. Thus, we consider the value of an effective Young modulus of the SAM E^*_{SAM} = 38 GPa as determined for the "model system" alkylthiol SAMs from a combined mechanics and electron transport study.[4] With these parameters, we estimate a = 2.3 nm (contact area = 16.6 nm^2) and δ = 0.2 nm. With a molecular packing density of 1.8 nm^2/molecule (see theory, below §6), we infer that about 10 molecules are measured in the Co-AzBT/PtIr junction.

We also checked that there is no short through the SAMs by comparing the I-Vs for the Co-AzBT/PtIr tip (Fig. 3, main text) with the typical I-Vs for a direct contact of the C-AFM tip on Co surface (Fig. S1), which show a current reaching the compliance limit of the preamplifier (here 10 μA) at V < 50 mV.

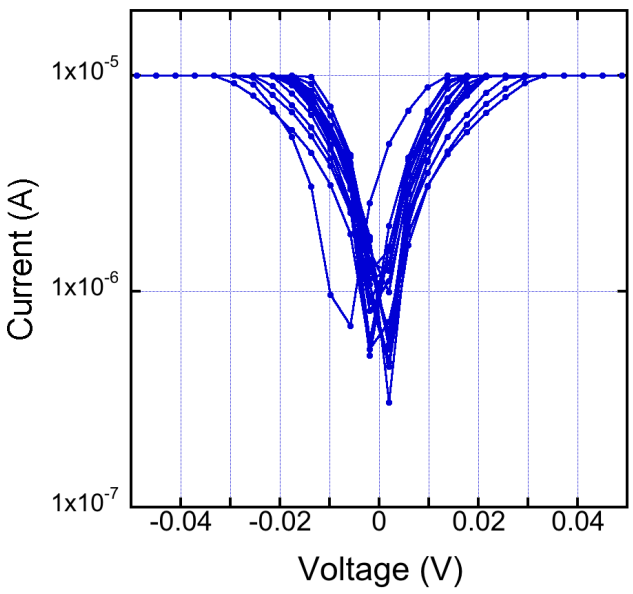

Figure S1. *Typical I-Vs (20 traces) for the direct contact of the PrIr C-AFM tip on a Co surface.*

4. XPS analysis of air-exposed cobalt

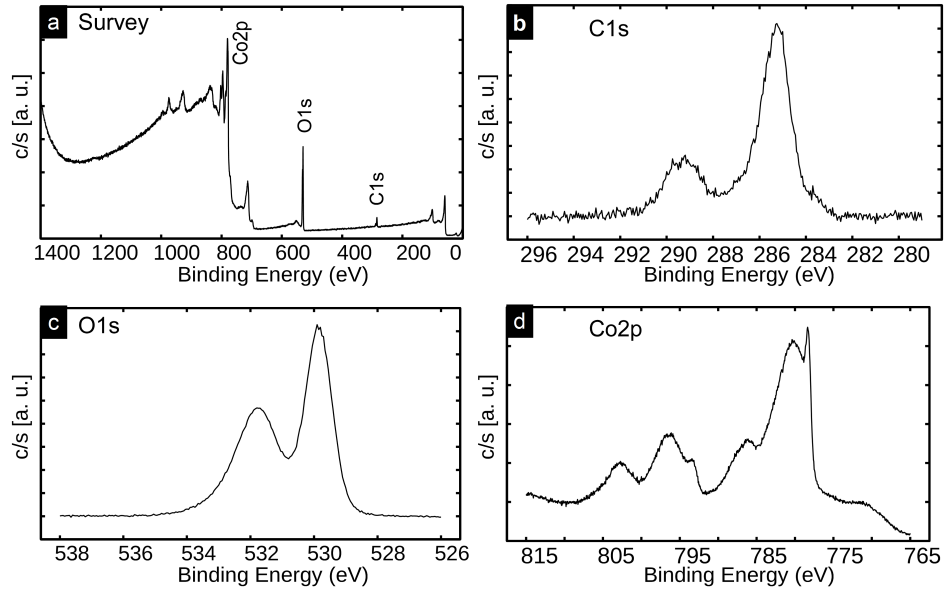

Figure S2. *XPS spectra of air-exposed cobalt:* ***(a)*** *survey,* ***(b)*** *C1s,* ***(c)*** *O1s,* ***(d)*** *Co2p.*

Spectra	Identification	Energy (eV)
C1s	C-C	285.2
C1s	C-O-C	286.3
C1s	C-C=O	289.3
O1s	CoO, Co_3O_4	529.8
O1s	C-O, $Co(OH)_2$	531.8
Co2p	Co metal 2p3/2	778.2
Co2p	CoO, Co_3O_4, $Co(OH)_2$ 2p3/2	780.3
Co2p	satellite	785.8
Co2p	Co metal 2p1/2	793.4
Co2p	CoO, Co_3O_4, $Co(OH)_2$ 2p1/2	796.4
Co2p	satellite	802.6

Table S1. *Identification of the peaks in the XPS analysis of air-exposed cobalt.*

Peak assignation from Refs. 14-18

5. XPS analysis of Co-AzBT SAM

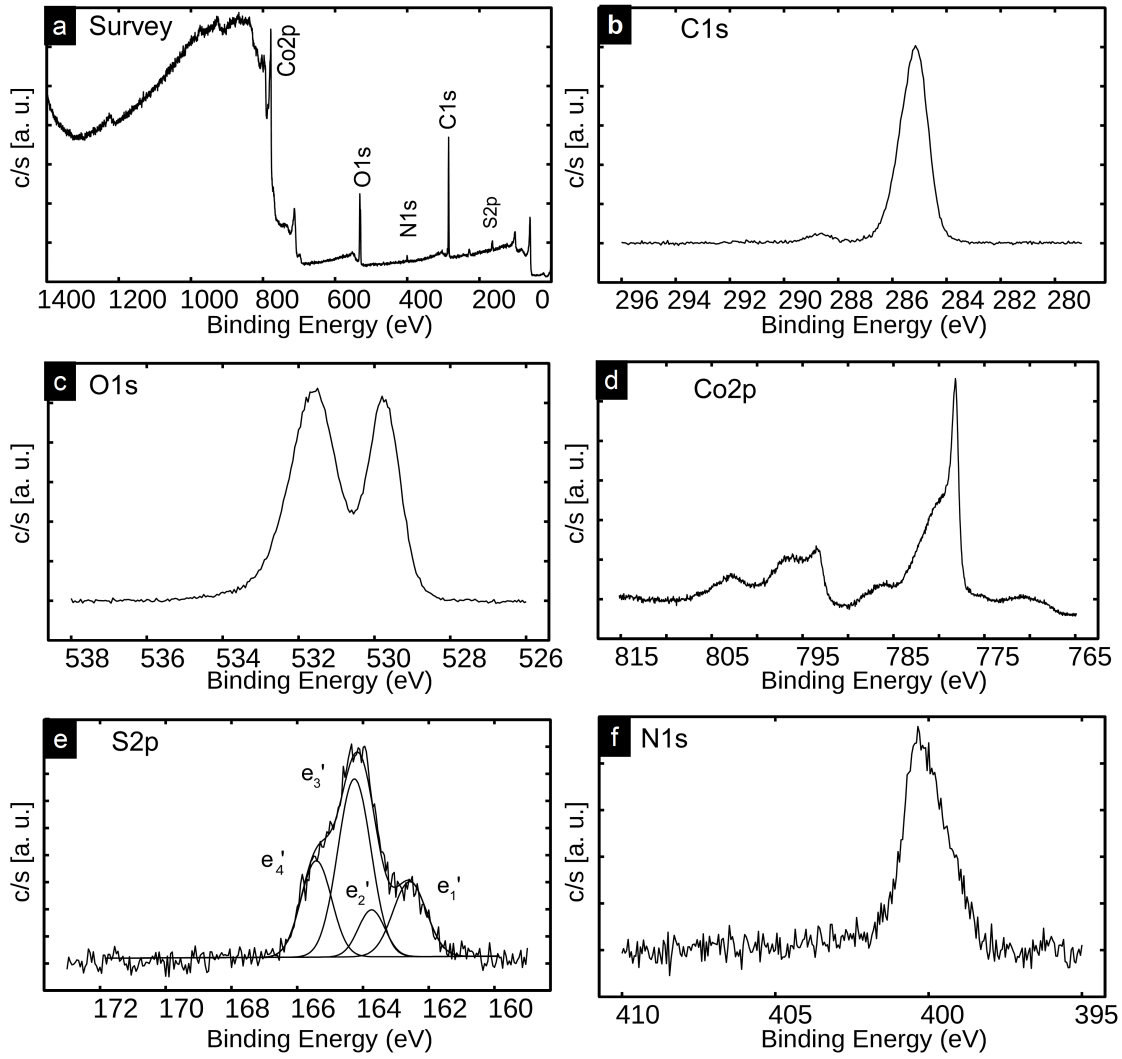

Figure S3. *XPS spectra of Co-AzBT:* ***(a)*** *survey,* ***(b)*** *C1s,* ***(c)*** *O1s,* ***(d)*** *Co2p,* ***(e)*** *S2p,* ***(f)*** *N1s.*

The O1s spectra is composed of two peaks at binding energies of 529.7 eV and 531.6 eV. These values are close to those observed by Chuang *et al.*[19] on cobalt surface exposed to air (529.5 eV and 530.8 eV). For these authors these peaks are associated to the oxidized cobalt. From the survey spectra (Fig. S3a), a smaller amount of oxygen is detected on Co-AzBT than on the air-exposed sample (Fig. S2a). For the Co-AzBT XPS analysis (Table S2), C1s peaks were observed approximately at the same

binding energy as on a cobalt surface exposed to the air without SAM (see Table S1). The first peak associated to C-C and C-S bonds and located at 285.1 eV was also observed on the sample of air-oxidized cobalt without SAM at 285.2 eV. However, the peak area is lower for the air-oxidized cobalt (divided by 4.8) compared to the sample with the SAM (Co-AzBT), with a peak area of 5192 (a.u.) and 1087 (a.u.) for Co-AzBT and air-oxidized cobalt respectively. So, the peak at 285.1 eV observed on Co-AzBT is a contribution of the carbon atoms of the AzBT molecule but also of the surface contamination. If we suppose that the contamination is the same for both the samples, we estimate that the peak observed at 285.1 eV on Co-AzBT is due to 21 % to the contamination and 79 % to the AzBT molecule grafted on the cobalt surface.

Spectra	Peak	Identification	Energy (eV)
C1s		C-C, C-S	285.1
C1s		C-O-C	285.6
C1s		C-C=O	288.7
O1s		CoO, Co_3O_4	529.7
O1s		C-O, $Co(OH)_2$	531.6
Co2p		Co metal 2p3/2	778.3
Co2p		CoO, Co_3O_4 2p3/2	780.5
Co2p		satellite	785.1
Co2p		Co metal 2p1/2	793.4
Co2p		CoO, Co_3O_4 2p1/2	796.4
Co2p		satellite	802.6
S2p	e_1'	CoS S2p3/2	162.6
S2p	e_2'	CoS S2p1/2	163.7
S2p	e_3'	CS S2p3/2	164.3
S2p	e_4'	CS S2p1/2	165.4
N1s		N in azobenzene	400.2

Table S2. *Identification of the peaks in the XPS analysis of Co-AzBT.*

Peak assignation from Refs. 14-18

6. Full theoretical methodology.

Co-AzBT self-assembled monolayers. First, the geometries of the isolated AzBT molecules are relaxed with forces below 0.01 eV/Å at the density functional theory (DFT) level using the Perdew-Burke-Ernzerhof (PBE) functional within the generalized gradient approximation (GGA),[20] as implemented in the QuantumATK software.[21, 22] The valence electrons are described within the LCAO approximation, with a double-zeta plus polarization basis set (DZP) whilst the core electrons are described by the norm-conserving Troullier-Martins pseudopotentials.[23] We use a density mesh cutoff of 100 Ha and

multipole boundary conditions to correct for the interaction between the single molecules introduced in a large unit cell and their images generated by the Periodic Boundary Conditions (PBC). The Co(111) surface is modeled by a slab of five layers with 11 × 3 cobalt atoms in each layer and lattice parameters a= 27.645 Å, b= 7.539 Å and α= 120°. This corresponds to a theoretical area per molecule of 180 $Å^2$ (see Fig. S4). A vacuum region of approximately 30 Å was introduced above the surface and 10 Å below it. The coordinates of the bottom three layers were kept fixed in the bulk lattice geometry while the two top layers were relaxed until the final forces acting on the atoms are less than 0.02 eV/Å. For this relaxation, we use the Perdew-Burke-Ernzerhof (PBE) functional with the spin generalized gradient approximation (SGGA),[20, 24] a double-zeta plus polarization basis set, a density mesh cutoff of 100 Ha and a (2×8×1) k-sampling.

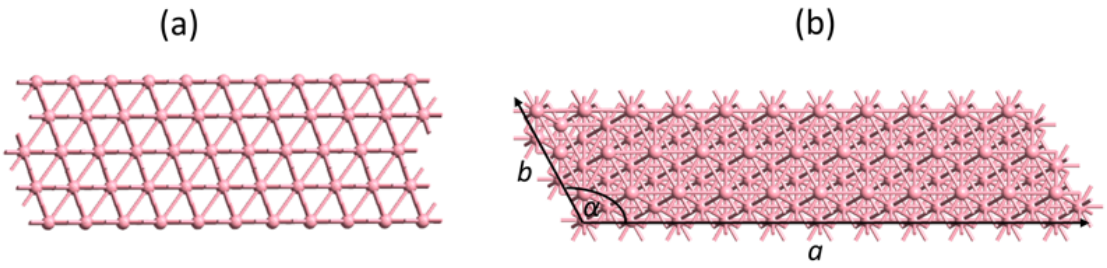

Figure S4. ***(a)*** *side and* ***(b)*** *top view of the Co (111) slab.*

Once the geometry is relaxed, the electronic structure and by extension the work function of the surface are computed using a 6×24×1 k-sampling, a 100 Ha mesh cutoff and a single-zeta plus polarization (SZP) basis set. We reduce the basis set here to be consistent with electronic structure computations achieved on larger systems such as SAMs and molecular junctions. For the resolution of Poisson's equation, Neumann (fixed potential gradient) and Dirichlet (fixed potential) were imposed on the left- and right-hand side of the slab, respectively, combined with periodic boundary conditions (PBC) in the in-plane directions. These mixed PBCs provide an alternative to the widely used slab

dipole correction.[25, 26] The Fermi energy is calculated initially for cobalt so that its energetic position ensures that the occupation of the density of states of the system equals the total number of electrons. Within this framework, we compute a work function of 3.78 eV for the Co(111) surface, a value too low compared to the experimental value of 5.00 eV.[27] This result is fully expected due to the use of short range localized atomic orbitals that induces an artificial push-back effect at the interface and thus reduces the metal work function. To solve this numerical problem, we added a layer of ghost atoms in the vacuum next to the surface to better describe the tail of the electron density, an approach already implemented in QuantumATK Q-2019.12-SP1.[21] Several tests have been performed in order to identify the nature of the ghost atoms, the converged distance from the top layer, the basis set and the pseudopotential that provide good accuracy at reasonable computational times. The obtained results indicate that the use of a layer of platinum ghost atoms described by medium basis sets and PseudoDojo pseudopotentials[28] at a distance of 1.6 Å from the top cobalt layer provides a work function of 5.07 eV, which is in very good agreement with the reported experimental value of 5.00 eV.[27]

To build the Co-AzBT SAMs, the molecules are tilted to fit the measured SAM thickness and then anchored on the cobalt surface through a sulfur atom. The SAM structures are optimized by relaxing the molecules forming the SAMS and the top two metal layers until forces are below 0.04 eV/Å. The exchange correlation SGGA.PBE functional has been used, with a (DZP) basis set for valence cobalt electrons (i.e., to describe the valence molecular orbitals), a (2×8×1) k-point sampling and a mesh cutoff of 100 Ha. The electronic structure and the SAM induced work function shift are then computed following the same method as used for the calculations on the bare cobalt surface, with a DZP basis set for the valence molecular orbitals. As described for the metal surface, a second ghost layer of gold atoms has been also positioned at -0.1 Å below the top molecular atoms to reduce the artificial push-back effect and prevent any artificial creation of bond dipole due to BSSE (Basis Set

Superposition Errors).[29] These two effects may induce errors larger enough to prevent a direct comparison between the work function shifts of the different systems.

The change in the work function upon SAM deposition, generally referred to as 'vacuum level shift' is well studied in the literature[30, 31] and has two main possible origins: (1) the intrinsic dipole moment of the molecules, reduced by the induced dipole arising from the depolarization effects triggered by the adjacent molecules;[32] and (2) the interfacial electronic reorganization upon formation of the Co-S bond resulting in a bond dipole in the vicinity of the interface. The apparent work function shift is then simply described as the sum of a molecular contribution ($\Delta\Phi_{SAM}$) and a bond dipole ($\Delta\Phi_{BD}$):

$$\Delta\Phi = \Delta\Phi_{SAM} + \Delta\Phi_{BD} \quad \text{(S4)}$$

The relative intensities of these two contributions depend on whether we adopt a neutral or a radical approach to describe the bonding of thiol to the metal surface. The neutral approach describes the adsorption as the replacement of a bond (the S-H bond) with a S-Co bond whereas the radical scenario considers the formation of a new covalent bond between the radical and the cobalt surface. For the sake of consistency with our previous studies,[33-35] we adopt here the 'radical scenario' for computing the molecular contribution and the bond dipole. To this end, we compute the electrostatic potential profile across a layer of radicals obtained by removing the cobalt atoms from the full system while keeping the same geometry for the molecular part; we then compute the energy difference between the left and right side of the layer, which corresponds directly to $\Delta\Phi_{SAM}$. The value of BD is obtained by subtracting $\Delta\Phi_{SAM}$ from the total shift. We note for sake of completeness that the amplitude of the work function shift can be related to the corresponding dipole moment by the Helmholtz equation:[36, 37]

$$\Delta\Phi = \mu / \varepsilon_0 A \quad \text{(S5)}$$

where μ is the dipole moment in the unit cell, projected along the axis normal to the surface, ε_0 is the vacuum permittivity and A is the area per dipole.

Co-AzBT molecular junctions. In a final stage, we add a second electrode on the top side of the molecular layer to build a single heterogeneous molecular junction Co-AzBT/Au. This second electrode is created by conserving the lattice parameters of the cobalt (111) surface and by converting the cobalt atoms to gold atoms to avoid problems related to lattice incommensurability. The choice of this type of electrode instead of a typical cobalt electrode is rationalized by two facts: (1) the measurements were performed with a PtIr tip, which is not a ferromagnetic material; and (2) the work function calculated for this top electrode is 4.81 eV, which is in good agreement with the experimental PtIr work function of 4.86 eV.[38] Note that this work function has been calculated by adding a ghost layer of gold atoms at a distance of 1.7 Å from the top gold layer of the second electrode.

A van der Waals contact is assumed between the molecular layer and the top electrode, with an interatomic distance determined as the sum of van der Waals radii of the hydrogen and gold atoms (2.86 Å). The electronic transport calculations of the Co-AzBT/Au junctions were performed by the combination of DFT to the Non-Equilibrium Green's Function (NEGF) formalism,[39] as implemented in QuantumATK Q-2019.12-SP1 package.[21, 22] This formalism has been widely recognized as a robust tool to rationalize the experimental results and predict new features and trends for charge transport in molecular junctions.[35, 40, 41] The exchange-correlation potential is described with the SGGA.PBE functional[20] whereas the Brillouin zone was sampled with a (3×12×100) k-sampling. We expand the valence electrons in a single zeta plus polarization basis set (SZP) for metal atoms (gold, gold ghost and cobalt), and a double zeta polarization basis set (DZP) for the other atoms. The core electrons are frozen and described by the norm-conserving Troullier−Martins pseudopotentials.[23] As for SAMs calculations, the platinum ghost atoms are described by a medium basis set and PseudoDojo potentials.

[28] The mesh cutoff was set to 80 Ha with a temperature of 300 K. These parameters have been carefully tested to ensure the convergence of the transmission spectrum.

The I-V characteristics have been calculated on the basis of the Landauer-Büttiker formalism,[42] that links the transmission spectrum to the current in a coherent transport regime. When a bias is applied, the current is calculated via the integration of the transmission spectrum within a bias window defined by a Fermi-Dirac statistics in the left and right electrodes:

$$I(V)=\frac{2e}{h}\int T(E)\left[f\left(E-\mu_L\right)-f\left(E-\mu_R\right)\right]dE \qquad \text{(S6)}$$

Where T(E) is the transmission spectrum, E the incident electron energy, f the Fermi-Dirac function $f(E-\mu)=[1+exp(E-\mu)/kT]^{-1}$, $\mu_{L/R}$ the chemical potential of the left/right electrode, e the elementary charge, h the Planck constant, k the Boltzmann constant and V the applied bias, with $|\mu_L - \mu_R| = eV$.

It is important to note that for an accurate estimation of the current, the transmission spectrum T(E) should be calculated in a self-consistent way for each bias. However, it is possible to obtain a reasonable approximation for the current at low bias by using the transmission spectrum at zero bias. This approximation is required here for our junctions with a large unit cell and a spin-polarized electrode because the self-consistent calculations become very time consuming. Accordingly, the current-voltage properties of Co-AZBT/Au were predicted by using the transmission calculated at equilibrium.

7. Junctions under bias

The computed ON/OFF ratios can be affected by the voltage drop profile across the junction. This voltage drop is hard to guess and should be computed theoretically. However, as explained in the methodology, these systems were computationally too heavy to be driven out of equilibrium. To get a qualitative idea of the ratio expected from theory, we thus integrated the equilibrium transmission by considering three extreme scenarios (see Fig. S5):

1. Under bias, one Fermi energy is fixed and the other one is driven up by $e|V|$.

2. Under bias, one Fermi energy is fixed and the other one is driven down by $-e|V|$.

3. Under bias, one Fermi level is driven up by $e|V|/2$ and the second level is driven down by $-e|V|/2$.

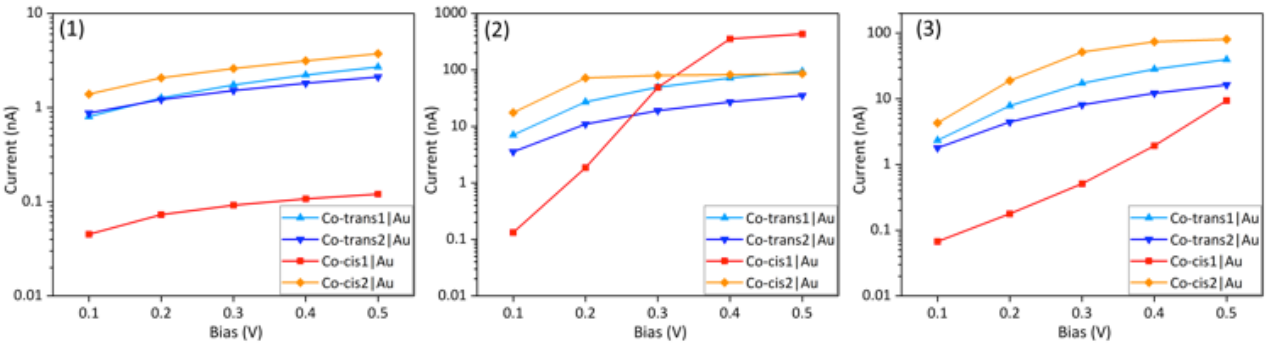

Figure S5. *Semilog scale plot of current (nA) versus bias when* ***(1)*** *a single Fermi level is driven up by* $e|V|$, ***(2)*** *a single Fermi level is driven down by* $-e|V|$ *and* ***(3)*** *one Fermi level is driven up by* $e|V|/2$, *and the second level is driven down by* $-e|V|/2$.

With our simplified methodology, the first and second scenario should give rise to a significant rectification as shown by the difference of the calculated I-V shapes between cases (1) and (2), because the HOMO and LUMO levels are not located symmetrically with respect to the Fermi energy (Fig. 6, main text), which is not seen experimentally. We thus conclude that the

symmetrical bias repartition, scenario (3), is more reasonable. Noteworthy, the higher slope that appears beyond 0.3V for *cis1* (see Fig S5-c) arises from the integration of the equilibrium transmission spectrum, which is clearly an approximation. Since this feature is not seen in the experimental curve, we speculate that the equilibrium transmission is not accurate beyond 0.3V and hence that our theoretical ratios are more accurate below 0.3V. We report the predicted ratios corresponding to the three scenarios in Table S3. In this low voltage range, the three scenarios predict ratios between *trans* and *cis1* between 14 and 53, hence with the same order of magnitude as the experimental values.

Scenarios	Ratios	0.1 V	0.2 V	0.3 V	0.4 V	0.5 V
(a)	Trans1/cis1	17.8	17.3	18.9	20.6	22.4
	Trans2/cis1	19.4	16.7	16.5	16.9	17.5
(b)	Trans1/cis1	53.0	14.6	1.0	0.2	0.2
	Trans2/cis1	26.8	5.9	0.4	0.2	0.2
(c)	Trans1/cis1	34.7	44.1	33.8	14.7	4.2
	Trans2/cis1	26.6	24.9	15.9	6.3	1.7

Table S3. *The calculated ON/OFF ratio between trans and cis1 forms for the different scenarios.*

REFERENCES

1. Shirley, D. A., High-Resolution X-Ray Photoemission Spectrum of the Valence Bands of Gold. *Phys. Rev. B* **1972,** *5*, 4709-4714.

2. Ulman, A., An introduction to ultrathin organic films : from Langmuir-Blodgett to Self-assembly. Academic press: Boston, 1991.

3. Parikh, A. N.; Allara, D. L.; Ben Azouz, I.; Rondelez, F., An intrinsic relationship between molecular structure in self-assembled n-alkylsiloxane monolayers and deposition temperature. *J. Phys. Chem.* **1994,** *98*, 7577-7590.

4. Engelkes, V. B.; Daniel Frisbie, C., Simultaneous nanoindentation and electron tunneling through alkanethiol self-assembled monolayers. *The Journal of Physical Chemistry B* **2006,** *110* (20), 10011-10020.

5. Smaali, K.; Desbief, S.; Foti, G.; Frederiksen, T.; Sanchez-Portal, D.; Arnau, A.; Nys, J. P.; Leclere, P.; Vuillaume, D.; Clement, N., On the mechanical and electronic properties of thiolated gold nanocrystals. *Nanoscale* **2015,** *7* (5), 1809-1819.

6. Thomas, L. Etude par microscopie à sond locale des propriétés électriques de monocouches auto-assemblées de molécules photo-commutables sur substrats ferromagnétiques. PhD thesis, University of Lille, 2018.

7. Necas, D.; Klapetek, P., Gwyddion: an open-source software for SPM data anylsis. *Central European Journal of Physics* **2012,** *10*, 181-188.

8. Horcas, I.; Fernández, R.; Gómez-Rodríguez, J. M.; Colchero, J.; Gómez-Herrero, J.; Baro, A. M., WSXM: A software for scanning probe microscopy and a tool for nanotechnology. *Rev. Sci. Instrum.* **2007,** *78* (1), 013705.

9. Cui, X. D.; Primak, A.; Zarate, X.; Tomfohr, J.; Sankey, O. F.; Moore, A. L.; Moore, T. A.; Gust, D.; Harris, G.; Lindsay, S. M., Reproductible measurement of single-molecule conductivity. *Science* **2001,** *294*, 571-574.

10. Cui, X. D.; Zarate, X.; Tomfohr, J.; Sankey, O. F.; Primak, A.; Moore, A. L.; Moore, T. A.; Gust, D.; Harris, G.; Lindsay, S. M., Making electrical contacts to molecular monolayers. *Nanotechnology* **2002,** *13*, 5-14.

11. Morita, T.; Lindsay, S., Determination of Single Molecule Conductances of Alkanedithiols by Conducting-Atomic Force Microscopy with Large Gold Nanoparticles. *J Am Chem Soc* **2007,** *129* (23), 7262-7263.

12. Johnson, K. L., *Contact Mechanics*. Cambridge University Press: New York, 1987.

13. WebElements, https://webelements.com.

14. Thermo Scientific XPS: knowledge base. https://xpssimplified.com/periodictable.php.

15. NIST, X-ray Phtoelectron Spectroscopy Data Base, V. 3.5, https://srdata.nist.gov/xps/.

16. Moulder, J. F.; Chastain, J., Handbook of X-ray photoelectron spectroscopy: A reference book of standard spectra for identification and interpretation of XPS data. Perkin-Elmer Corporation: 1992.

17. Hoertz, P. G.; Niskala, J. R.; Dai, P.; Black, H. T.; You, W., Comprehensive investigation of self-assembled monolayer formation on ferromagnetic thin film surfaces. *J. Am. Chem. Soc.* **2008,** *130* (30), 9763-9772.

18. Devillers, S.; Hennart, A.; Delhalle, J.; Mekhalif, Z., 1-Dodecanethiol Self-Assembled Monolayers on Cobalt. *Langmuir* **2011,** *27*, 14849-14860.

19. Chuang, T. J.; Brundle, C. R.; Rice, D. W., Interpretation of the x-ray photoemission spectra of cobalt oxides and cobalt oxide surfaces. *Surface Science* **1976,** *59* (2), 413-429.

20. Perdew, J. P.; Burke, K.; Ernzerhof, M., Generalized Gradient Approximation Made Simple. *Phys. Rev. Lett.* **1996,** *77* (18), 3865-3868.

21. *QuantumATK Q-2019.12-SP1*, Synopsis QuantumATK, www.synopsys.com/silicon/quantumatk.html.

22. Smidstrup, S.; Stradi, D.; Wellendorff, J.; Khomyakov, P. A.; Vej-Hansen, U. G.; Lee, M.-E.; Ghosh, T.; Jónsson, E.; Jónsson, H.; Stokbro, K., First-principles Green's-function method for surface calculations: A pseudopotential localized basis set approach. *Physical Review B* **2017,** *96* (19), 195309.

23. Troullier, N.; Martins, J. L., Efficient pseudopotentials for plane-wave calculations. *Physical Review B* **1991,** *43* (3), 1993-2006.

24. Smidstrup, S.; Markussen, T.; Vancraeyveld, P.; Wellendorff, J.; Schneider, J.; Gunst, T.; Verstichel, B.; Stradi, D.; Khomyakov, P. A.; Vej-Hansen, U. G.; Lee, M.-E.; Chill, S. T.; Rasmussen, F.; Penazzi, G.; Corsetti, F.; Ojanperä, A.; Jensen, K.; Palsgaard, M. L. N.; Martinez, U.; Blom, A.; Brandbyge, M.; Stokbro, K., QuantumATK: an integrated platform of electronic and atomic-scale modelling tools. *Journal of Physics: Condensed Matter* **2019,** *32* (1), 015901.

25. Neugebauer, J.; Scheffler, M., Adsorbate-substrate and adsorbate-adsorbate interactions of Na and K adlayers on Al(111). *Physical Review B* **1992,** *46* (24), 16067-16080.

26. Natan, A.; Kronik, L.; Shapira, Y., Computing surface dipoles and potentials of self-assembled monolayers from first principles. *Applied Surface Science* **2006,** *252* (21), 7608-7613.

27. Michaelson, H. B., The work function of the elements and its periodicity. *J. Appl. Phys.* **1977,** *48* (11), 4729-4733.

28. van Setten, M. J.; Giantomassi, M.; Bousquet, E.; Verstraete, M. J.; Hamann, D. R.; Gonze, X.; Rignanese, G. M., The PseudoDojo: Training and grading a 85 element optimized norm-conserving pseudopotential table. *Computer Physics Communications* **2018,** *226*, 39-54.

29. Van Dyck, C.; Bergren, A. J., Large Built-In Fields Control the Electronic Properties of Nanoscale Molecular Devices with Dipolar Structures. *Adv. Electron. Mater.* **2018,** *4* (5), 1700656.

30. Heimel, G.; Romaner, L.; Zojer, E.; Bredas, J.-L., The Interface Energetics of Self-Assembled Monolayers on Metals. *Accounts of Chemical Research* **2008,** *41* (6), 721-729.

31. Heimel, G.; Rissner, F.; Zojer, E., Modeling the Electronic Properties of π-Conjugated Self-Assembled Monolayers. *Adv. Mater.* **2010,** *22* (23), 2494-2513.

32. Cornil, D.; Olivier, Y.; Geskin, V.; Cornil, J., Depolarization Effects in Self-Assembled Monolayers: A Quantum-Chemical Insight. *Adv. Funct. Mater.* **2007,** *17* (7), 1143-1148.

33. Crivillers, N.; Liscio, A.; Di Stasio, F.; Van Dyck, C.; Osella, S.; Cornil, D.; Mian, S.; Lazzerini, G. M.; Fenwick, O.; Orgiu, E.; Reinders, F.; Braun, S.; Fahlman, M.; Mayor, M.; Cornil, J.; Palermo, V.; Cacialli, F.; Samori, P., Photoinduced work function changes by isomerization of a densely packed azobenzene-based SAM on Au: a joint experimental and theoretical study. *Phys. Chem. Chem. Phys.* **2011,** *13* (32), 14302-14310.

34. Osella, S.; Cornil, D.; Cornil, J., Work function modification of the (111) gold surface covered by long alkanethiol-based self-assembled monolayers. *Physical Chemistry Chemical Physics* **2014,** *16* (7), 2866-2873.

35. Rodriguez-Gonzalez, S.; Xie, Z.; Galangau, O.; Selvanathan, P.; Norel, L.; Van Dyck, C.; Costuas, K.; Frisbie, C. D.; Rigaut, S.; Cornil, J., HOMO Level Pinning in Molecular Junctions: Joint Theoretical and Experimental Evidence. *J. Phys. Chem. Lett.* **2018,** *9* (9), 2394-2403.

36. Schuhmann, D., The model of two parallel condensers and the application of the Helmholtz formula to adsorption of polar surfactants from aqueous solutions. *Journal of Electroanalytical Chemistry and Interfacial Electrochemistry* **1986,** *201* (2), 247-261.

37. Evans, S. D.; Urankar, E.; Ulman, A.; Ferris, N., Self-assembled monolayers of alkanethiols containing a polar aromatic group: effects of the dipole position on molecular packing, orientation, and surface wetting properties. *J Am Chem Soc* **1991,** *113* (11), 4121-4131.

38. Lee, N. J.; Yoo, J. W.; Choi, Y. J.; Kang, C. J.; Jeon, D. Y.; Kim, D. C.; Seo, S.; Chung, H. J., The interlayer screening effect of graphene sheets investigated by Kelvin probe force microscopy. *Appl. Phys. Lett.* **2009,** *95* (22), 222107.

39. Brandbyge, M.; Mozos, J.-L.; Ordejón, P.; Taylor, J.; Stokbro, K., Density-functional method for nonequilibrium electron transport. *Phys. Rev. B* **2002,** *65* (16), 165401.

40. Schmaus, S.; Bagrets, A.; Nahas, Y.; Yamada, T. K.; Bork, A.; Bowen, M.; Beaurepaire, E.; Evers, F.; Wulfhekel, W., Giant magnetoresistance through a single molecule. *Nature Nanotech*. **2011,** *6*, 185-189.

41. Van Dyck, C.; Geskin, V.; Kronemeijer, A. J.; De Leeuw, D. M.; Cornil, J., Impact of derivatization on electron transmission through dithienylethene-based photoswitches in molecular junctions. *Phys. Chem. Chem. Phys*. **2013,** *15* (12), 4392-4404.

42. Büttiker, M.; Imry, Y.; Landauer, R.; Pinhas, S., Generalized many-channel conductance formula with application to small rings. *Physical Review B* **1985,** *31* (10), 6207-6215.